N132D: Chandra and XMM-Newton X-ray Imaging and Spectral Analysis

Paul P. Plucinsky, Adam R. Foster, Terrance J. Gaetz (SAO), William P. Blair (JHU), Richard J. Edgar, Diab Jerius, Daniel J. Patnaude, & Randall K. Smith (SAO)

Abstract

We have used archival data from the Chandra X-ray Observatory and XMM-Newton to study the X-ray morphology and spectra of the Large Magellanic Cloud SNR N132D. The X-ray emission is dominated by the interaction of the forward shock with the swept-up interstellar material. Narrow band images centered on the prominent emission lines of S, Ar, and Fe-K indicate that the emission from these elements is centrally-concentrated in the remnant. The X-ray spectra are of sufficient statistical quality that multiple component models are necessary to provide adequate fits. We have extracted spectra from multiple locations around the shell of the remnant and the interior. For the interior spectra, the low-energy part (E<2.0 keV) of the spectrum can be fit with two thermal components with characteristic temperatures of kT~0.3 and kT~0.8 keV. The high energy part of the spectrum (E>2.0 keV) requires a thermal component with kT~4.5 keV to explain the continuum and the line ratios at Ar, Ca, & Fe-K. The centrally-concentrated morphology, relatively high temperature, and abundances argue that this component is produced by ejecta heated by the reverse shock.

X-ray Image Analysis

N132D was observed by Chandra for 89ks in 2006. Figure 1 displays the broad, soft, and hard images, and a three-color image. The pixels are 0.5x0.5 arcsec^2 and a Gaussian smoothing with a radius of 3 pixels has been applied. The emission in the soft band dominates, indicating that most of the emission comes from the shock interaction with swept-up ISM. The three color image indicates that the emission is harder on average toward the South than in the North. N132D has been observed by XMM-Newton 43 times over the course of the mission as a calibration target. We have selected a subset of these observations that are suitable for imaging analysis with a total exposure of 1.3 Ms. Figure 2 shows the MOS1+MOS2 data in four bands centered on the O, S, Ar, and Fe-K line complexes. The pixel size is 2.4x2.4 arcsec^2 and a Gaussian smoothing with a radius of three pixels has been applied. The morphology of the O emission is similar to the overall morphology of the remnant, but the S, Ar, and Fe-K are more concentrated towards the center of the remnant. Figure 3 shows the Fe line and continuum images and a hardness ratio map from the Chandra data. In each panel, events are binned into 2x2 arcsec^2 pixels, and the broad band (0.35-8.0 keV) contours are overlaid. In the counts images, green=1 count, red=2 counts, and white=3 counts. The upper left panel contains the band centered on the 6.7 keV Fe-Kα line. There are about 64 cts in the Fe-Kα line in the central part of the remnant. The upper right and lower left panels contain the adjacent continuum bands at lower energy and higher energy respectively. The lower right panel contains the hardness ratio 4.0-6.1 keV/0.35-4.0 keV. This image shows where the kT=4.5 keV plasma contributes more to the total emission. The 4.0-6.1 keV band is typically less than 0.5% of the 0.35-4.0 keV band.

Figure 1: Chandra Broad, 3 Color, Soft and Hard Images

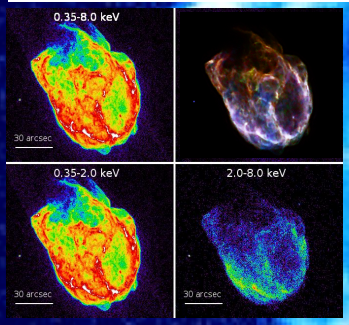

Figure 2: XMM Narrow Band Images

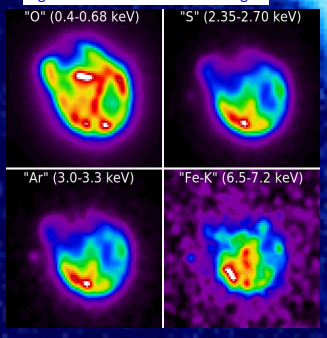

Figure 3: Chandra Narrow Band and Ratio Images

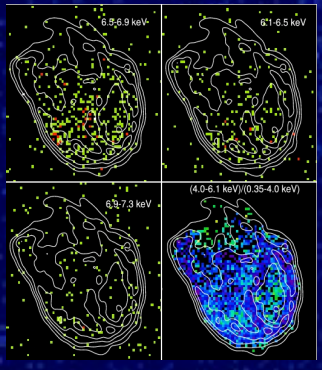

N132D Background

N132D is the brightest X-ray SNR in the LMC, with a luminosity of L_x(0.3-10.0 keV)~1.0x10^{38} ergs/s. N132D was classified as an O-rich remnant based on optical spectra (Lasker 1978). The remnant has a complicated morphology in X-rays with many bright filaments which appear along the line-of-sight to the interior of the remnant and several faint protrusions ahead of the brightest parts of the shock. The southwestern part of the remnant appears to have a semi-circular shell but the northeastern part of the remnant has a fragmented and decidedly non-spherical structure. The H_α data match the bright shell seen in the X-rays, indicating pre-shock material photoionized by the X-ray/EUV emission. The Spitzer 24μm image (Tappe et al. 2006) shows the outer shell as well, indicating heated, swept-up dust. A dense CO cloud has been mapped just to the south of the remnant (Banas et al. 1997, Sano et al. 2015). The X-ray, optical, and IR morphology are consistent with a remnant expanding into a cavity, and the bright shell emission indicates the interaction between the main blast wave and the cavity wall in the south (Hughes 1987).

Morse et al. (1996) estimated an age of ~3,000 yr based on the expansion of the O-rich knots. HST Faint Object Spectrograph (FOS) showed lines of C, O, Ne, & Mg but no evidence of Si, S, Ca, & Ar. Blair et al. (2000) suggested that the progenitor may have had an O-rich mantle which did not mix with the innermost ejecta layers. France et al. (2009) claim detection of weak Si IV emission, in addition to C and O, from an HST Cosmic Origins Spectrograph (COS) spectrum. Early XMM results based on only 23 ks of data (Behar et al. 2001) show a centrally concentrated morphology for the Fe-K emission, while the O-K, Ne-K and Fe-L emission trace the outer bright parts of the shell. Vogt & Dopita (2010) constructed a 3D map of the [O III] filaments to show that the O ejecta form a ring 12 pc in diameter inclined ~25 degrees from the line of sight and estimated an age of 2,500 yr. They concluded from this that the reverse shock has propagated all the way back to the center of the remnant. Borkowski et al. (2007) used the high-resolution image from Chandra to conclude that some of the O emission seen in X-rays was co-spatial with some of the O filaments seen in the optical. The picture that emerges from the existing data is that of a remnant of a core-collapse SNe expanding into a cavity created by its precursor in which the reverse shock has propagated through most or all of the ejecta.

Chandra Spectral Analysis

We extracted spectra from five locations around the outer shell as indicated by the regions in Figure 4. We fit the data with a model of galactic absorption (fixed to 6.25x10^{19} cm^{-2}) and LMC absorption (free) modifying a two component model, a thermal component (a vnei model in XSPEC) and a power-law component. The temperature for the vnei component and the power-law index and normalization were allowed to vary but tied together for the the five spectra. The LMC absorption and normalization for the vnei component were allowed to vary for each of the spectra. The source and background spectra were modeled simultaneously and the C statistic was used. Our background model consisted of a sky background component (dominated by the transfer streak of N132D itself) and a detector background component. The five spectra are show in Figure 6 in different colors. A single spectral model with the exception of a different value of the LMC absorption and vnei normalization fits the data well. The fit results are tabulated in Table 1. Emission lines from Mg, Si, and S are visible in the spectra.

We extracted spectra from annular and circular regions, excluding the northern part of the regions as indicated in Figure 5. The data were fit with a similar model as above, a two component absorption model but instead of a vnei plus a power-law, we used two vnei components. The source and background spectra for the three regions are shown in Figures 7, 8, & 9. The fit results are tabulated in Table 2. The thermal components have temperatures approximately equal to 0.3 keV and 0.9 keV. The brightest regions of the remnant in annuli #2 & #3 are affected by pileup, whereas annulus #1 and the shell spectra are unaffected by pileup. Pileup suppresses the observed count rate in the 0.5-1.0 keV band and enhances the rate in the 1.0-2.0 keV band. The fit for the Ann #1 region has the smallest residuals. The fit for the Ann #2 region has significant residuals around 6.4 keV and the fit for the Ann #3 region has large residuals around 6.4 keV. There also appears to be a high energy continuum in the Ann #3 spectrum that is not well modeled. These results indicate that the majority of the Fe-K emission and the high energy emission is coming from the interior of the remnant, consistent with the imaging results.

Fig 4: Chandra Shell Spectral Extractions

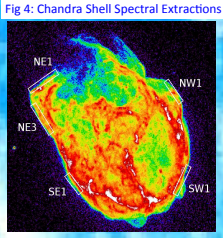

Fig 5: Chandra Annular Spectral Extractions

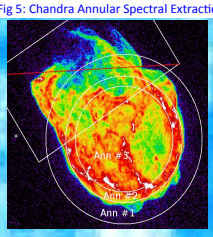

XMM Spectral Analysis

We have used a number of different exposures from calibration observations of N132D from the MOS2 and the PN cameras, totaling roughly 150ks for MOS2 with the thin and medium filters, and 160ks of PN data with the thin filter. A similar amount of data was excluded from our analysis due to the presence of pileup in the large and full window modes for both instruments. The data was reprocessed and extracted for the full remnant using SAS 13.5, which includes the new MOS contamination model. Instrumental backgrounds were modeled using a combination of power laws and gaussians as suggested in the ESAS manual. A background normalization factor was introduced for each detector and allowed to vary. The background model is constrained by the signal above 9keV.

By using a model for N132D consisting of 2 line-broadened thermal plasma models (bvapec), we were able to reproduce the spectrum between 3 and 12 keV, providing an acceptable fit (C-Stat = 5338 for 5393 DOF) simultaneously to the PN and MOS spectra (see Figure 10). The abundances of Fe, Ca and Ar were freed, and the results were all found to remain close to the solar values (Ar: 0.75+/- 0.08, Ca: 1.07+/-0.13, Fe: 0.91+/-0.09). This is significantly enhanced from the typical LMC values of 1/3 solar. The temperatures of the two bvapec components are 0.9+/-0.04 and 4.5+/-0.5keV. The exact temperature of the hot component varies depending on the exact spectral region which is fitted, but there is consistently a hot component.

We have then refitted the spectrum, replacing the high temperature component with a bremsstrahlung and gaussians. This allows separate measurement of the temperature implied by the ratios of the He-like Kα and Kβ lines, and the H-like Lyα. Figure 11 shows that the resulting line ratios are consistent with a plasma with kT between 3.8 and 5.0keV, while the continuum component is constrained to be above 3.5keV. The consistency of this reveals that there is a significant hot plasma component within N132D, which is responsible for the bulk of the Fe K line emission. Figure 12 shows the addition of a 4.5 keV thermal component to the Chandra annulus #3 spectrum.

Fig 10: XMM pn & MOS2 Spectrum of N132D

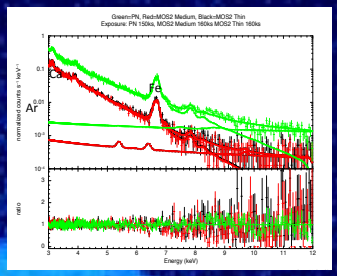

Fig 11: Theoretical and Observed Line ratios from Fe K

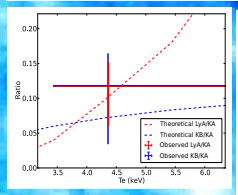

References

Banas, K.R. et al. 1997, ApJ, 480, 60
Behar, E. et al. 2001, A&A, 365, L242
Blair, W.P. et al. 2000, ApJ, 537, 667
Borkowski, K.J. et al. 2007, ApJ, 671, L45
France, K. et al. 2009, ApJ, 707, L27
Hughes, J.P. 1987, ApJ, 314, 103
Lasker, B.M. 1978, ApJ, 223, 109
Morse, J.A. et al. 1996, AJ, 112, 509
Sano, H. et al. 2015, arXiv:1503.04390
Tappe, A. et al. 2006, ApJ, 653, 267
Vogt, F., & Dopita, M.A. 2011, APSS, 331, 521

Conclusions

The imaging results from both Chandra and XMM show that the high Z elements (S, Ar, & Fe) are concentrated toward the interior of the remnant. The Chandra spectra show that the vast majority of the Fe-K emission comes from the interior of the remnant. The XMM spectral data indicate that the abundances of Ar, Ca & Fe are enhanced by a factor 2-3 times typical LMC abundances for a plasma close to collisional ionization equilibrium. The XMM spectral data can be fit with continuum temperatures of 0.9 and 4.5 keV and the ratios of the He-like Kα and Kβ lines, and the H-like Lyα line of Fe are consistent with a temperature of 4.5 keV. A hot ejecta component may be responsible for the bulk of the Fe K emission. A long observation with high angular resolution is necessary to unequivocally detect and characterize an ejecta component in N132D.

Fig 6: Chandra Shell Spectral Fits

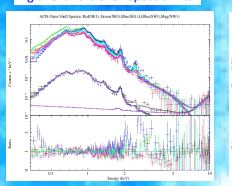

Fig 8: Chandra Ann #2 Spectral Fit

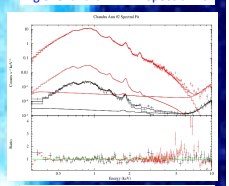

Fig 7: Chandra Ann #1 Spectral Fit

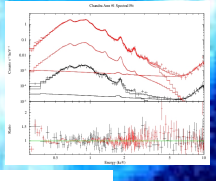

Fig 9: Chandra Ann #3 Spectral Fit

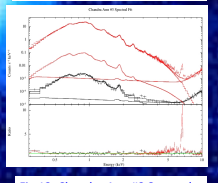

Table 1: Chandra Spectral Fit Results for the Shell

Spectral model tbabs(Gal) * tbvarabs(LMC) *(vnei + pow)

		Spectrum N_H (LMC) [x10^{21} cm^{-2}]
kT = 0.30 keV [0.29,0.31]	NE1	1.79 [1.73,2.04]
n_et = 1.33 x10^{13} cm^{-3} s	NE3	1.81 [1.77,2. 07]
index= 3.31[2.99,3.35]	SE1	3.77 [3.72,4.08]
Cstat=3343	SW1	2.79 [2.74,3.08]
DOF=3951	NW1	2.00 [1.93,2.26]

Table 2: Chandra Spectral Fit Results for the Annular Regions

Spectral model tbabs(Gal) * tbvarabs(LMC) *(vnei + vnei)

Spectrum	N_H(LMC) [x10^{21}]	kT1(keV)	n_et1(cm^{-3} s) [x10^{13}]	kT2(keV)	n_et2(cm^{-3} s) [x10^{13}]	Cstat	DOF
Ann#1	1.85	0.25	3.31	0.77	4.15	1719	1313
Ann#2	1.85	0.28	3.31	0.93	4.15	2724	1313
Ann#3	1.85	0.27	3.31	0.97	4.15	4667	1313
Ann#3 with 4.54 keV component	1.85	0.30	3.31	0.80	4.15	3013	1307

Fig 12: Chandra Ann #3 Spectral Fit with 4.5 keV component